Environmental and Ecological Statistics
https://doi.org/10.1007/s10651-023-00560-z

Modelling local climate change using site-based data

Isabella Morlini[1] · Maria Franco-Villoria[2] · Stefano Orlandini[3]

Received: 19 July 2022 / Revised: 23 March 2023 / Accepted: 21 April 2023

Abstract

In the context of the ongoing United Nations Framework Convention on Climate Change (UNFCCC) process, it seems important to focus attention not only on global mean surface air temperature (GSMT) but also on the climate of specific regions in order to gain insights into the dynamics of the changes, the timescales of the periodic components, the local trends and the relationships between climatic variables in the region of interest. This is important for scientists as well as for policymakers. This paper provides an analysis of the changes in local air temperature and precipitation depth in exceptionally long observational records and examines the relationships between these two variables. The focus is on monthly values. Temperature maximum, minimum, range, and cumulative precipitation depth are considered. The wavelet analysis shows that the scale of variation is different for temperature and precipitation and that the behavior of the temperature range values diverges from the behavior of the minimum and maximum values. The timescale of important changes in the long-term trend is, however, similar. Results also suggest that the main mode of variability is persistent through time in the series of temperature maximum, minimum, and range but not in precipitation depth. This is a clear evidence of climate change. All series show variances that change over time and are, as expected, nonstationary. The analysis of the wavelet coherence shows that the relationship between precipitation and temperature evolves through time, and its intensity varies considering different time scales. The association between these climatic variables is particularly strong in the last decade. Is it noteworthy that the analysis of the coherence suggests that temperature is leading to rain and not the other way around. This highlights the impact of global warming on the hydrologic cycle and on related human activities.

Isabella Morlini, Maria Franco-Villoria and StefanoOrlandini have contributed equally to this work.

Handling Editor: Luiz Duczmal

Extended author information available on the last page of the article

Published online: 03 June 2023

Keywords Air tempearture · Climate interactions · Precipitation depth · Wavelet analysis

1 Introduction

The subject of climate change usually focuses attention on global mean surface air temperature both for analyzing temperature change (Easterling et al. 1996; Hansen and Lebedeff 1987; Hansen et al. 2010; Thompson et al. 2009; Ozbay and Toker 2021) and for estimating relationships between temperature and climate forcing mechanisms like carbon dioxide and solar irradiance (Hansen et al. 1981; Simmons et al. 2010; De Laat and Maurellis 2004; Broecker 2012; Boucher and Reddy 2008). However, it is the change on regional and local scales that affects people directly, and the knowledge of this change is essential for the development of adaptation strategies and policy makers intervention (Sutton et al. 2015). Geophysical local time series are often generated by complex systems of which we know little about, and predictable behavior in such systems, like trends and periodicities are therefore of great interest [see, among others, Woody et al. (2020)]. In this paper, we examine historical variations in local surface air temperature and precipitation depth using data from the Geophysical Observatory of the University of Modena and Reggio Emilia (Italy). These data can provide uncommon evidence of the long-term trend and of the relationships between temperature and precipitation, which are hard to find in any global investigation due to the scarcity of long observed (and not simulated) time series. Discrete and continuous wavelets are used to characterize the time series and to study the association between temperature and precipitation, to compare the features of these climatic variables and to detect the abrupt shifts in both cyclic and trend dynamics. The tools of the discrete and continuous wavelet transforms (Torrence and Compo 1998; Percival and Walden 2000; Ruskal et al. 1992; Chui 1992), the wavelet spectra, coherence, and phase offer a comprehensive assessment of the characteristic modes of variability of climate system forcing and of the scale-based relationships between natural climate variables (Kumar and Foufoula-Georgiou 1993; Gambis 1992; Gao and Li 1992). In addition, short-term variations in local surface temperature and rain can be associated with internally generated natural climate variability and external climate forcing, while long-term variations are strongly related to human-induced changes only (Gallegati 2018). In particular, the research questions addressed in this work, are:

1. Which frequencies contribute the most to the variability of the series? Do the periodicities remain constant or evolve over time? Are these periodicities the same in temperature and precipitation?
2. How does the long-term trend evolve over time? Is there a point of an important significant discontinuity?
3. At which timescales, if any, do temperature and precipitation have a common behavior? Has the association between these two variables changed in the last decade? Which variable influences the other one?

Giving an answer to these questions means systematically weather changes and the relationships between variations in temperature and precipitation. Even though the annual cumulative precipitation depth and the annual maximum and minimum temperature do not show evident dynamics in time, the study of climate change requires consideration and comparison of both the internal variability in the local system and the behavior due to global development. Wavelet analysis is used here to separate the contribution of these two factors by reconstructing the original time series as a sum of detailed components, each of which corresponds to an oscillating component with a different period that can be associated with local variations, and a smooth component showing the long-term trend, that can be associated to a global dynamic.

The rest of the paper is organized as follows. Section 2 illustrates the data and methods. Section 3 reports and discusses the results of the statistical analyses. Conclusions and directions for future research are reported in Sect. 4.

2 Data and methods

2.1 Data

The monthly time series of maximum and minimum air temperature *Tmax* and *Tmin* and temperature range *Trange* (°C) and cumulative precipitation depth *PMM* (mm), displayed in Fig. 1, are obtained from uninterrupted daily observations collected from 01/01/1861 to 12/31/2020 at the Geophysical Observatory of the University of Modena and Reggio Emilia (latitude 44.6474° N, longitude 10.9293° E, elevation 76.50 m asl), Modena, Italy. These long term in situ observations (160 years, 1920 monthly observations per series) are not affected by in-homogeneities caused by changes in instrumentations, station moves, different observing practices (for example, different formulas for calculating the minimum and the maximum) or different observations time. Therefore, observed variability is due to changes in the local and global environment and can be related to global CO_2 as well as to variations in the local development. *Tmax* and *Tmin* are defined as the maximum and minimum daily values in the month, respectively, while *Trange* is the monthly average of the daily temperature range values. While changes in the maximum and minimum temperatures are strongly associated with changes in the average temperature, temperature range provides additional information for observing climate variability and change (Braganza et al. 2003, 2004). For this reason, in this study we also consider the monthly average of the difference between daily maximum temperature and minimum temperature, as it has been shown to be an important meteorological indicator associated with global climate change (Qu et al. 2014; Easterling et al. 1997; Leathers et al. 1998; Karl et al. 2004; Sun et al. 2006). *PMM* is defined as the cumulative precipitation depth in the month. There are 9 missing values in precipitation in 1943 that are inputed using cubic spline interpolation.

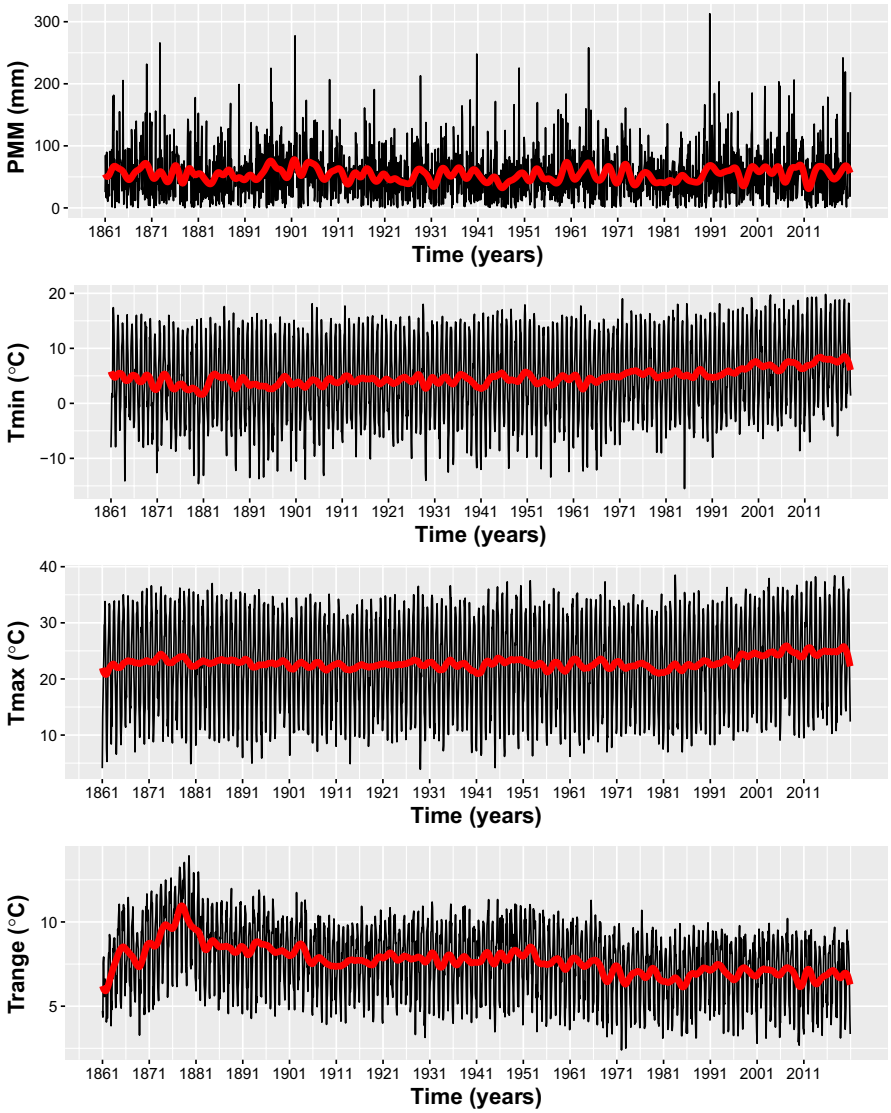

Fig. 1 Time series plot of monthly cumulated *PMM*, minimum (*Tmin*), maximum (*Tmax*) and range (*Trange*) temperature values. The red line on each plot displays the long-term trend (S_4) obtained from the wavelet anlaysis

2.2 Methods

To extract information and to identify scales of variation in the series we perform a wavelet analysis. In order to uncover the different characteristics of the series, we apply both discrete and continuous wavelets. We use a modified version of the classic Daubechies wavelet for the discrete analysis (Daubechies 1988; Akansu et al.

1992; Akansu and Smith 1995; Mallat 1999) called "least asymmetric" (LA), and the Morlet wavelet for the continuous analysis. The LA filter is a common choice in practical applications (see, for example, Elayouty et al. 2016). The Daubechies orthogonal wavelets with different orders are the most widely used discrete wavelets in geophysics since they are compactly supported (Daubechies 1992; Lau and Weng 1995) and the behavior of the signal at infinity does not play any role. While Daubechies wavelets may be preferred for synthesis and data compression, continuous Morlet wavelets may be preferred for scale analysis. The advantage of using the Morlet wavelet over the other continuous wavelets is due to its complex nature that is able to detect both time dependent amplitude and phase for different frequencies exhibited in the time series (Lau and Weng 1995). For a comparison of different continuous wavelets in an ecological context we refer to Mi et al. (2005). All the analyses are carried out with `R` (R Core Team 2021), using the R packages `wavelets` (Aldrich 2020), `biwavelet` (Gouhier et al. 2021) and an advanced version of the latter (Schulte 2019), available at the website of the author.

We first use the discrete wavelet transform (DWT) to perform a spectral analysis assuming stationarity, in order to partition the variance of the series into its different oscillating components with different frequencies (periods) and to detect which frequencies contribute the most to the variance of the series. We then use the discrete wavelet for a non-stationary analysis by performing a local time-scale decomposition of the series and estimating the spectral characteristics as a function of time (Lau and Weng 1995; Torrence and Compo 1998). Directly related to these methods is the approach proposed by Nason et al. (2000), where time-varying variance is accounted for, and a time-varying spectrum is computed, assuming first-order stationarity. An example where this method is used in a climatology context is Beaulieu et al. (2020). Rather than overthrowing existing methodology, the work provides an additional complementary tool for time series without trends. Recent work by McGonigle et al. (2022), who also analyzes a temperature data set, shows that the approach of Nason et al. (2000) can be extended to smooth trends and proposes a wavelet-based framework to model time series exhibiting time-varying first and second-order structure. The trend is considered to be a deterministic smooth function representing long-term (low frequency) patterns or systematic variations in the time series. Further, we use the continuous wavelet transform (CWT) approach that is more suited for the extraction of local time-scale or time-frequency information and is characterized by a well-defined relationship between frequency and scale (Daubechies 1992). As shown in Cazelles et al. (2008), while discrete wavelets are more appropriate for the representation of the process on appropriate bases and the relationship between scale and frequency in this approach has less meaning, the main feature of continuous wavelets is the time-frequency decomposition with the optimal trade-off between time and frequency resolution, which permits investigation of the temporal evolution of aperiodic and transient processes. Last, we use the continuous wavelet coherence for a bi-variate analysis of the time series, in order to detect and quantify the non stationary association between precipitation and temperature.

2.2.1 Wavelet transform

The wavelet transform decomposes a signal over dilated and translated functions of the so called "mother wavelet" $\psi(t)$ (Percival and Walden 2000) that can be expressed as a function of two parameters, one for the time position, τ, and one for the scale of the wavelet, a. More formally, wavelets are defined as $\psi_{a,\tau}(t) = a^{-1/2}\psi\left(\frac{t-\tau}{a}\right)$. The wavelet transform of a time series $x(t)$ of length T ($t = 1, \ldots, T$), with respect to a chosen mother wavelet is performed as follows:

$$W_x(a,\tau) = \frac{1}{\sqrt{a}} \int_{-\infty}^{\infty} x(t)\psi^*\left(\frac{t-\tau}{a}\right)dt = \int_{-\infty}^{\infty} x(t)\psi^*_{a,\tau}(t)dt \tag{1}$$

where $*$ denotes the complex conjugate form. The wavelet coefficients $W_x(a,\tau)$ represent the contribution of the scales (the a values) to the signal at different time positions τ. The wavelet transform can be though of as a cross-correlation of a signal $x(t)$ with a set of wavelets of various widths or scales a at different time positions τ. The wavelet function is not arbitrary. It is rather normalized to have unitary variance so that $\int |\psi(t)|^2 dt = 1$ and it verifies $\int \psi(t)dt = 0$. The wavelet decomposition is therefore a linear representation of the series where the variance is preserved. The original series can be recovered by using the following inverse transform:

$$x(t) = \int_{-\infty}^{\infty}\int_{0}^{\infty} \frac{1}{a^2} W_x(a,\tau)\psi_{a,\tau}(t)\,dt\,da \Big/ \int_0^{\infty} \|\Phi(f)\|^2/f\,df \tag{2}$$

where $\Phi(f)$ denotes the Fourier transform of $\psi(t)$. Therefore, the wavelet transform is just a linear filter whose response function is given by the wavelet function. By means of (2), the original series can be reconstructed by integrating over all scales and locations. However, the integration can be limited over a chosen range of scales $a_1 - a_2$, to perform a band-pass filtering of the original time series in this chosen range. This analysis is called multiresolution analysis (MRA). In the discrete domain, the scale and shift parameters are discretized as $a = a_0^m$ and $\tau = n\tau_0$, with $a_0 > 1$ and $\tau_0 \neq 0$ to restrict the values of the parameters to a discrete sublattice [see Daubechies (1988)]. The wavelets are also discretized, as follows:

$$\psi_{m,n}(t) = a_0^{-m/2}\psi\left(\frac{t - n\tau_0}{a_o^m}\right) \tag{3}$$

where n and m are integer values. The discrete wavelet transform and its inverse transform are defined as follows:

$$W_{m,n} = \int_{-\infty}^{\infty} \psi^*_{m,n}(t)x(t)dt, \tag{4}$$

$$x(t) = k_\psi \sum_m \sum_n W_{m,n}\psi_{m,n}(t) \tag{5}$$

where k_ψ is a constant value for normalization. The function $\psi_{m,n}(t)$ provides sampling points on the scale-time plane that are linear sampling in the time direction but logarithmic in the scale (a-axis) direction. The scales are on a dyadic base since a_0 is chosen as $a_0 = 2^j$ where j is an integer value. This is analogous to the use of a set of narrowband filters in conventional Fourier analysis.

2.2.2 Mother wavelet

In our application, for the discrete analysis we use a modified version of the Daubechies wavelet, called least asymmetric (LA). This wavelet is the orthogonal wavelet with a phase response that most closely resembles a linear phase filter; this allows to align the filtered series in time with the original series. The wavelets in the least asymmetric family have compact support and are indexed by a parameter N proportional to the regularity since, as N increases, the wavelet becomes smoother. In our application, $N = 8$. The wavelet is defined as follows:

$$\psi(t) = \sum_{k=-\infty}^{\infty} \beta_k \sqrt{2}\phi(2t - k) \tag{6}$$

where $\phi(t)$ is a compactly supported scaling function, $\phi(t) = \sum_{k=-\infty}^{\infty} \alpha_k \sqrt{2}\phi(2t - k)$ for the progression $\{\alpha_k\}$, k real integer, satisfying the following conditions for all integers $N \geq 2$:

$$\alpha_k = 0 \text{ if } k < 0 \text{ or } k > 2N \tag{7}$$

$$\sum_{k=-\infty}^{\infty} \alpha_k \, \alpha_{k+2m} = \delta_{0m}, \text{ for all integers } m \tag{8}$$

where δ_{0m} is the Kronecker delta,

$$\sum_{k=-\infty}^{\infty} \alpha_k = \sqrt{2} \tag{9}$$

$$\sum_{k=-\infty}^{\infty} \beta_k k^m = 0, 0 \leq m \leq N - 1 \tag{10}$$

where $\beta_k = (-1)^k \alpha_{-k+1}$. The function (6) satisfies the N vanishing moments condition $\int \psi(t) t^m dt = 0$, for all integers $0 \leq m \leq N - 1$. This last property has important implications for applications since it ensures that fine-scale wavelet coefficients will only be large where a function or its derivatives have singularities (Daubechies 1992). Another important feature is that the wavelet compact bases are capable of representing various classes of functions more efficiently than Fourier bases (Donoho et al. 1994). If we consider, as an example, a piecewise continuous function, many Fourier basis functions are needed to represent the discontinuities accurately and the effects of these basis functions will be global. On the other hand,

wavelets will be able to represent the discontinuities more efficiently and at the same time they will be local and will not affect the global representation. The DWT has some limitations in terms of sample size (it has to be a power of two), and the starting point and filter choice can have an impact on the wavelet transform of the series. Instead, we use the maximum overlap DWT (MODWT); this is no longer an orthogonal transformation which means a higher computational cost ($\mathcal{O}(T \log T)$ as opposed to $\mathcal{O}(T)$ for the DWT), but without the issues that the DWT has (Percival and Walden 2000). In either case, for a given level of decomposition J, the original series can be re-expressed as the sum of a number of wavelet details components $\boldsymbol{D}_j$, $j = 1, \ldots, J$ and a smooth component $\boldsymbol{S}_J$. The wavelet detail $\boldsymbol{D}_j$ can be seen as a time series related to variations in the original time series at a scale of 2^{j-1} months, $j = 1, \ldots, J$, while the smooth component $\boldsymbol{S}_J$ can be interpreted as a time series related to variations in X at scale of 2^J and higher, so one could think about $\boldsymbol{S}_J$ as the long-term trend. The filtering performed assumes the time series to be a portion of a larger periodic sequence with period T, so we might expect boundary effects at the beginning and end of the series.

For the continuous analysis we utilize the mostly used Morlet mother function, defined as follows:

$$\psi(t) = \pi^{-1/4} e^{i\omega_0 t} e^{-t^2/2} \tag{11}$$

where ω_0 is the non dimensional frequency taken to be 6 to satisfy the admissibility conditions. For $\omega_0 = 6$, the second term in the Fourier transform of (11):

$$\Phi(\omega) = e^{(-\omega-\omega_0)^2/2} - e^{-\omega^2/2} e^{-\omega_0^2/2} \tag{12}$$

is so small that it can be neglected in practice and the Morlet wavelet can be consequently considered as a modulated Gaussian waveform. Another characteristic of the Morlet wavelet is that the relation between the frequency f and the scale parameter a can be derived analytically and $\frac{1}{f} = \frac{4\pi a}{\omega_0 + \sqrt{2+\omega_0^2}}$ with ω_0 the central angular frequency of the wavelet ($\omega_0 = 2\pi f_0$). With ω_0 around 2π the scale a is inversely proportional to the frequency f. This greatly simplifies the interpretation of the wavelet analysis and one can replace, in all results, the scale a by the frequency f or the period $1/f$. With $\omega_0 = 6$ the Fourier period p_F is almost equal to the scale, since $p_F = 1.03a$ (Torrence and Compo 1998).

2.2.3 Wavelet power spectra and cone of influence

Following the previous paragraph, the scale a is replaced by the frequency f in the notation that follows. Considering the wavelet transform of a time series $x(t)$ defined in (1), we can obtain the local wavelet power spectrum, which gives the indication of how volatile a time series is across different time scales, as follows:

$$S_x(f, \tau) = \|W_x(f, \tau)\|^2. \tag{13}$$

Since we are dealing with finite-length time series, errors will occur at the beginning and end of the wavelet power spectrum as the transform assumes the data is cyclic.

As the wavelet gets closer to the edge of the time series, parts of it exceed the edge and thus the values of the wavelet transform are affected creating boundary effects. The affected region increases in extent as the scale a (or the frequency f) increases. This zone where edge effects are present is called "cone of influence" and the spectral information in the cone lacks in accuracy and should be interpreted with caution. The Fourier spectrum of a series, assuming stationarity, can be related to the global wavelet power spectrum which is defined as the averaged variance contained in all wavelet coefficients of the same frequency f or scale a:

$$\bar{S}_x(f) = \frac{\sigma_x^2}{T} \int_0^T \|W_x(f,\tau)\|^2 dt \tag{14}$$

with σ_x^2 the variance of the time series $x(t)$ and T the length of the series. Another interesting computation is the mean variance at each time location, obtained by averaging the frequency components:

$$\bar{s}_x(\tau) = \frac{\sigma_x^2 \pi^{1/4} \tau^{1/2}}{\int_0^\infty \|\Phi(f)\|^2 / f df} \int_0^\infty \left(\frac{1}{f}\right)^{1/2} \|W_x(f,\tau)\|^2 dt \tag{15}$$

where $\Phi(f)$ is the Fourier transform of $\psi(t)$. This quantity can also be filtered in a chosen frequency band (or range of scales) to perform a multiresolution analysis.

2.2.4 Wavelet coherence and phase difference

For the bi-variate analysis, we use the wavelet coherence. In Fourier analysis, the coherence is used to determine the association between two time series. The coherence function is a direct measure of the correlation between the spectra of two time series. To quantify the relationship between two non stationary series, one can compute the wavelet coherence. Following Torrence and Webster (1999), we define the wavelet coherence between two time series $x(t)$ and $y(t)$ as the cross spectrum $W_{x,y}(f,\tau) = W_x(f,\tau) W_y^*(f,\tau)$ with * denoting the complex conjugate, normalized by the spectrum of each series:

$$R_{x,y}(f,\tau) = \frac{\|\langle W_{x,y}(f,\tau)\rangle\|}{\|\langle W_{x,x}(f,\tau)\rangle\|^{1/2} \|\langle W_{y,y}(f,\tau)\rangle\|^{1/2}} \tag{16}$$

where the symbol $\langle\rangle$ denotes a smoothing operator in both time and scale. $R_{x,y}(f,\tau)$ is bounded in [0, 1]. The smoothing is performed by a convolution with a constant length window function both in the time and frequency direction (Chatfield 1989). For the Morlet wavelet, the most suited smoothing operator having similar footprint as the wavelet, is given in Torrence and Webster (1999). It is

$$\left(W_{x,y}(f,\tau) * c_1^{\frac{-t^2}{2f^2}} \right)\Big|_f$$

for the frequency and

$$(W_{x,y}(f,\tau) * c_2\Pi(0.6a))\Big|_{\tau}$$

for time, where c_1 and c_2 are normalization constants and Π is the rectangle function. The factor 0.6 is an empirically determined scale decorrelation length. In practice both convolutions are done directly and the normalization coefficients are determined numerically. The advantage of these quantities based on wavelets is that they vary in time and can also detect transient correlations between two series. The wavelet coherence provides information about at which temporal location and frequency two non stationary time series are linearly correlated. The quantity $R_{x,y}(f,\tau)$ can be interpreted as the proportion of power of $x(t)$ explained by the linear relation with the power of $y(t)$ at a particular time and frequency band. It has the same meaning of a square correlation coefficient between two time series. Since the Morlet wavelet is complex, we may also obtain information about the possible delay in the relationship, that is information about which variable is leading the other one, by computing the phase difference. The analysis of the phase or out of phase relationship allows us to get insights into the asymmetric association between the two series, which could be useful for making hypotheses about possible causal relationships. The phase difference is defined as follows:

$$\psi_{x,y}(f,\tau) = \tan^{-1}\frac{\mathfrak{I}\big(\langle W_{x,y}(f,\tau)\rangle\big)}{\mathfrak{R}\big(\langle W_{x,y}(f,\tau)\rangle\big)}, \tag{17}$$

where $\mathfrak{I}$ indicates the imaginary part and $\mathfrak{R}$ the real part. The phase difference varies cyclically between $-\pi$ and π over the duration of the component waveforms. Positive values suggest that is $x(t)$ leading $y(t)$ while negative values suggest the opposite situation. Values close to zero indicate that the relationship between the two series, if present, is symmetric.

2.2.5 Significance level

One can test whether the wavelet-based quantities, that is the spectra or coherence, observed at a particular time for a particular scale, are real features and not due to a random process with the same Markov transitions as the original time series. In our application, we perform hypothesis testing using the existing R functions written by Schulte (2019) and available at the author's website. The functions are an advanced version of the `biwavelet` R package. Regarding the wavelet spectrum, one can compare the estimated sample spectrum with a background noise spectrum. To make such comparisons, statistical tests such as the point-wise (Torrence and Webster 1999), area-wise (Maraun and Kurths 2004; Maraun et al. 2007), geometric (Schulte et al. 2015), and cumulative area-wise (Schulte 2016a) can be implemented. The point-wise significant test proposed by Torrence and Webster (1999) is the first and still mostly used method that allows placing wavelet analysis in a statistical hypothesis testing framework. In the point-wise approach, the statistical significance of wavelet quantities associated with points in a wavelet spectrum is assessed individually, without considering the correlation structure among wavelet

coefficients. For wavelet power spectra of climate time series, theoretical red-noise spectra are the preferred noise background spectra against which sample wavelet power spectra are tested. Regarding coherence, more recent Monte Carlo methods are used to estimate the background noise spectra (Schulte 2016b; Grinsted et al. 2004). We apply both the point-wise approach and the cumulative area-wise test developed by Schulte (2019). The second approach overcomes some drawbacks of the first one addressed in literature, like the frequent generation of many false positive results because of the simultaneous testing of multiple hypotheses (Maraun et al. 2007; Schulte et al. 2015) and the occurrence of spurious results in clusters because of the correlations of the wavelet coefficients.

3 Analysis

3.1 Discrete wavelet and multiresolution analysis

Multiresolution analysis (MRA) permits a very detailed analysis by separating the signal into components at different scales. We apply the MODWT with dyadic scale, allowing us to decompose variations in the monthly series at scales of 1, 2, 4 months and so on. As introduced in Sect. 2.2.2, for a fixed level of decomposition J, the original time series $\boldsymbol{X}$ can be reconstructed based on the wavelet coefficients as $\boldsymbol{X} = \sum_{j=1}^{J} \boldsymbol{D}_j + \boldsymbol{S}_J$, where $\boldsymbol{X}$ is the time series vector of length T. The analysis of monthly data with $J = 4$ gives a sequence of results which relate to variations at scales of 1, 2, 4, and 8 months. The value $J = 4$ was chosen to explore changes in the data within the year (seasonality in particular), which we expect to be more relevant than variations on a multiannual scale (that could be investigated using a greater J) for this kind of data. We considered greater values of J (not shown here) to ensure that the dominant modes of variability had been identified with $J = 4$. Extracting signal components at different resolutions amounts to decomposing variations in the data on different time scales, or equivalently in different frequency bands (different rates of oscillation). Accordingly, one can visualize signal variability at different scales, or frequency bands simultaneously. Detail components $\boldsymbol{D}_j$ become progressively smoother since, in terms of frequency, the frequencies contained in the components become progressively lower. Figure 2 reports, for each time series, the distribution of the estimated wavelet variances $\hat{\nu}^2_{\boldsymbol{X}}(a_j), j = 1, \ldots, 4$, calculated as the variance of the wavelet coefficients $\{W_{a_j,t}\}$ at that scale. The estimated wavelet variance at scale a_j can be calculated as:

$$\hat{\nu}^2_{\boldsymbol{X}}(a_j) = \frac{1}{M_j} \sum_{t=1}^{M_j} W^2_{a_j,t}$$

where M_j is the number of coefficients not affected by boundary conditions at scale j. It is interesting because it provides a decomposition of the time series variance $\sigma^2_{\boldsymbol{X}}$ on a scale by scale basis.

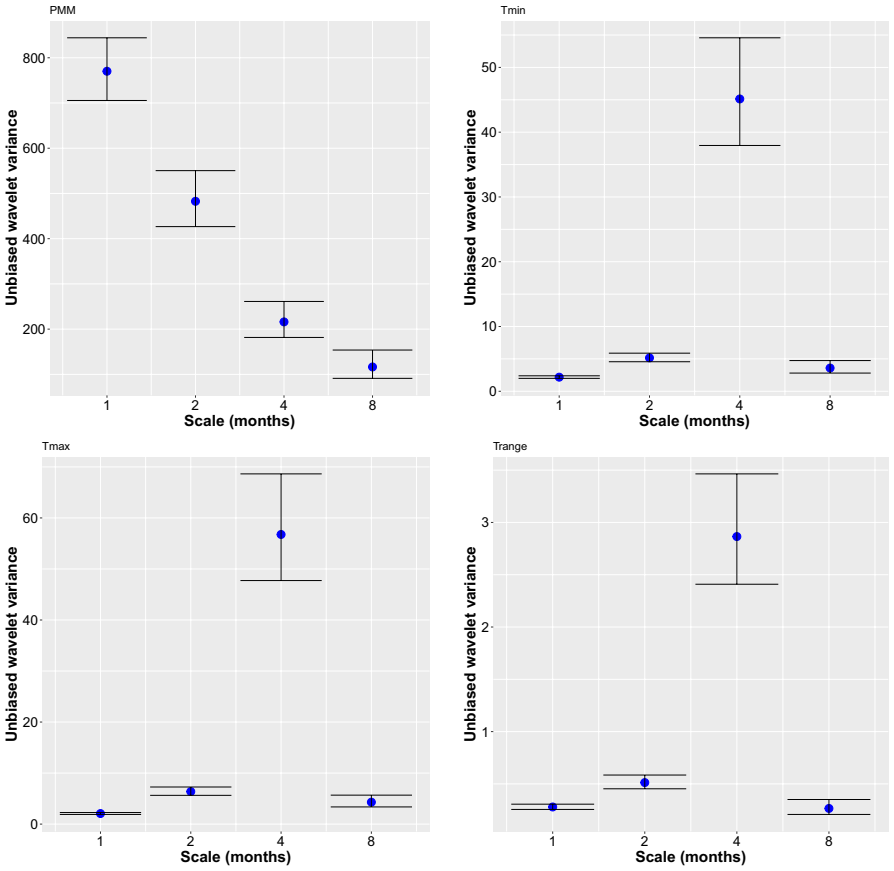

Fig. 2 Wavelet variance decomposition of monthly cumulated *PMM* (top left) and monthly *Tmin* (top right), monthly *Tmax* (bottom left) and monthly average *Trange* (bottom right)

The analysis reveals that temperature and precipitation have a different periodicity. While for the minimum, the maximum and the temperature range the main periodic component (that is, the scale contributing the most to the variance of the series) is clearly 4 months and the periodicity is thus close to the seasonality, for rain intensity the main periodic component is one month. Figures 3, 4, 5, and 6 show the wavelet detail series $\boldsymbol{D}_3$ for *PMM*, *Tmin*, *Tmax* and *Trange*, corresponding to the scale of 4 months previously detected as the main periodic component for temperature. As outlined before, we can think of $\boldsymbol{D}_3$ as the seasonal component in the data. We also report the wavelet detail series $\boldsymbol{D}_1$ (Fig. 7) for *PMM*, as it is the main responsible for the variability in the *PMM* time series.

The analysis reveals that the main oscillating component is nearly constant through time, both in amplitude and time location, for *Tmin*, *Tmax* and *Trange*. On the contrary, the seasonal behavior of the rain intensity is quite irregular, with more frequent peaks in the last four decades. It is hard to identify changing

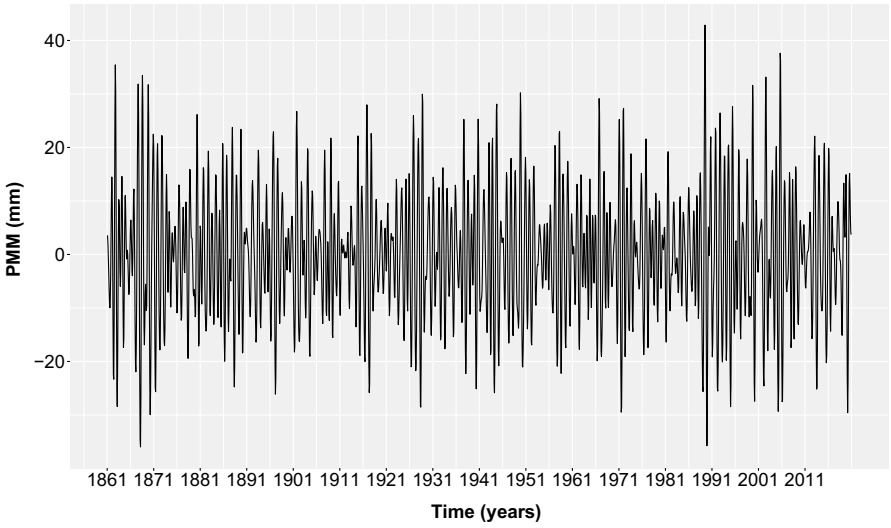

Fig. 3 Time series plot of $\boldsymbol{D}_4$ for monthly cumulated *PMM* (scale 4 months)

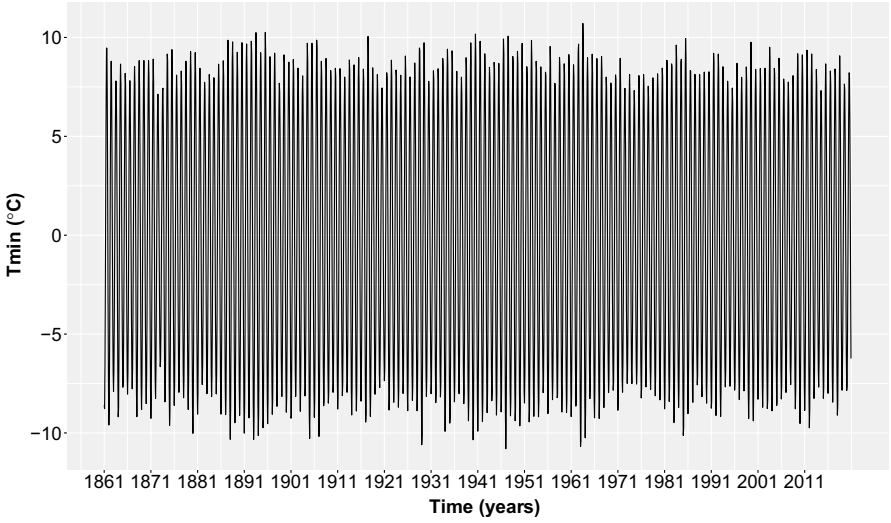

Fig. 4 Time series plot of $\boldsymbol{D}_4$ for monthly *Tmin* (scale 4 months)

behavior or any specific time evolution in the considered period (Fig. 3). However, if we analyze the monthly pattern $\boldsymbol{D}_1$ (Fig. 7) we note that extreme peaks are present in some years all over the observed period but the last two decades are characterized by the absence of nearly-zero amplitudes, quite frequent in the past years, and relative higher amplitudes of the oscillating component. We may conclude that, even though the seasonal behavior of the rain intensity doesn't show

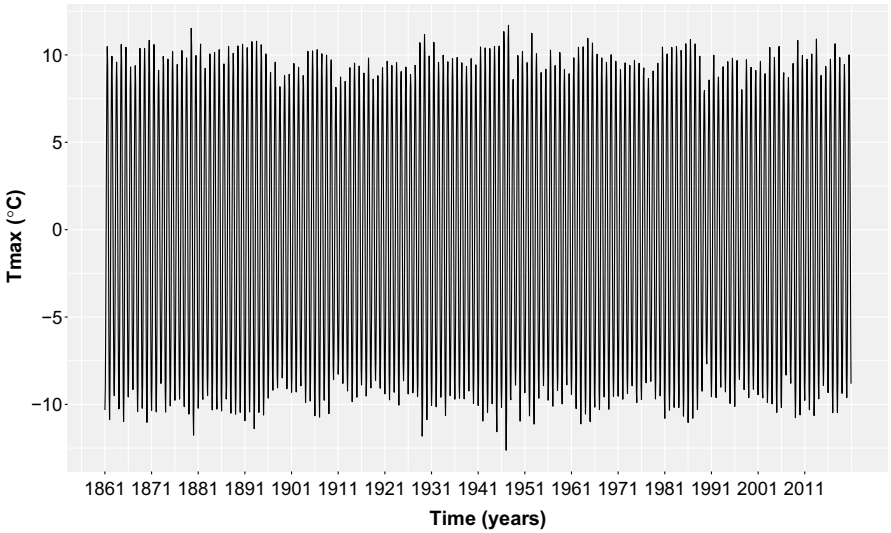

Fig. 5 Time series plot of $\boldsymbol{D}_4$ for monthly *Tmax* (scale 4 months)

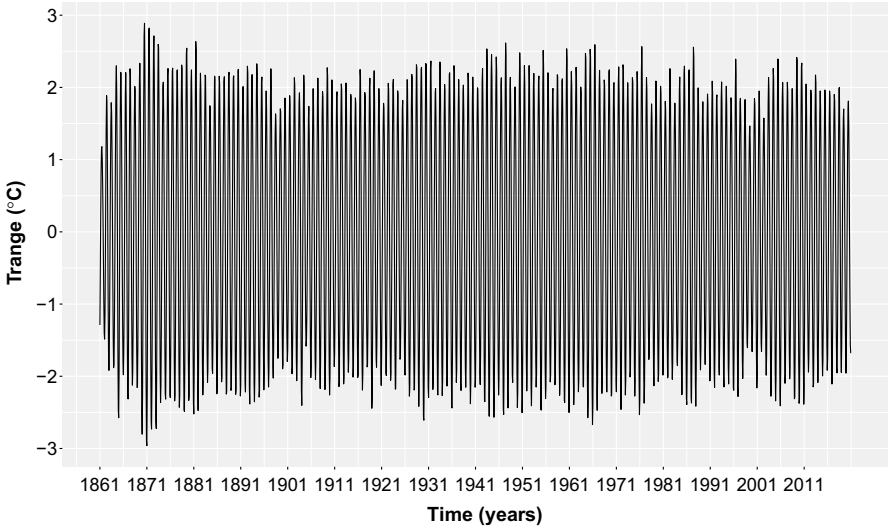

Fig. 6 Time series plot of $\boldsymbol{D}_4$ for monthly *Trange* (scale 4 months)

an evident change in the last decades, the monthly behavior has indeed changed in the mode of variability. The long term trend, that is the $\boldsymbol{S}_4$ wavelet smooth for all series, is shown in Fig. 8.

We note an evident change in the trend component in all temperature series from around 1960 and a decrease in *Trange* over time. While both the minimum and the maximum temperature start increasing as ever before, the range temperature starts

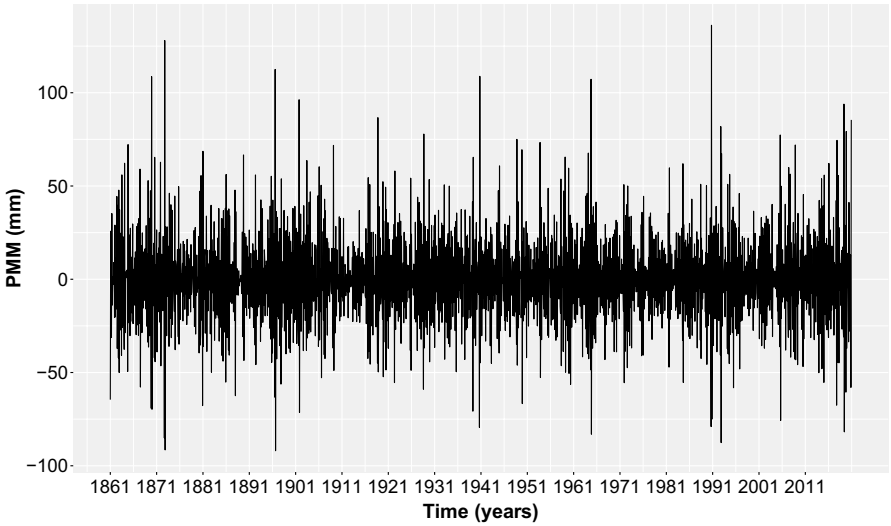

Fig. 7 Time series plot of $\boldsymbol{D}_1$ for monthly cumulated *PMM* (scale 1 month)

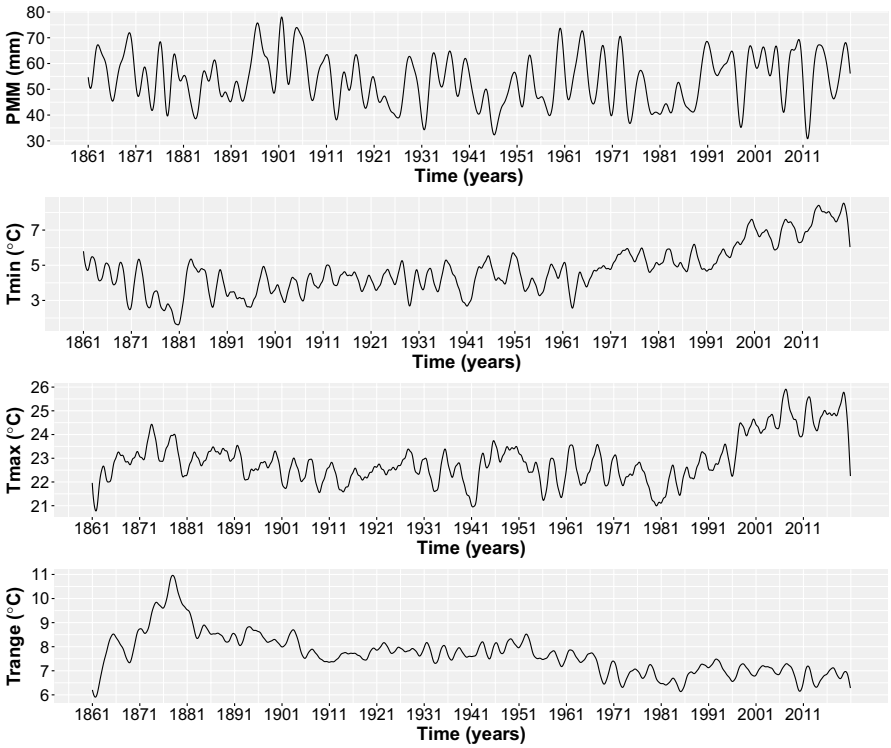

Fig. 8 Time series plot of $\boldsymbol{S}_4$ for all series (scales 16 months and higher)

decreasing. Recent changes in the dynamics of the range temperature can be related to climate changes due to anthropogenic forcing (Stone and Weaver 2002, 2003; Dai et al. 1999). The reduction of the range is associated to larger increases in minimum temperature than maximum temperatures over the same period and this difference has been attributed in literature to a number of factors such as urban heat, land use change, aerosols and greenhouse gases changes in solar irradiance (Braganza et al. 2004; Makowski et al. 2008). Different regions may be affected by different factors. In this study, we do not consider the possible anthropogenic causes but we find that, for the region of interest, temperature changes are indeed present in the last 50 years, as supported by other local and global studies (Makowski et al. 2008). The large negative trend of the range temperature is an important meteorological indicator that reflects the instability of the weather, very unlikely to have occurred due to internal variability or external climate forcing but rather associated to global dynamics related to human-induced changes.

3.2 Time-dependent wavelet variance

The wavelet analysis reported in the previous section assumes variability to be constant over time. While the wavelet variance can be useful as a first estimate to identify the main scale of variation, a better understanding of the process can be gained by means of the time-dependent wavelet variance when nonstationarity is suspected. As an alternative, some works based on the wavelet periodogram have been proposed to perform formal testing on stationarity (Nason 2013) and detect multiple change points (Korkas and Fryzlewicz 2017). We can explore the time-dependent wavelet variance at scale a_j by choosing a smoothing window N_s and by estimating the wavelet variance as a moving average of squared wavelet coefficients (note that the mean for the coefficients is zero) as follows:

$$\hat{v}^2_{\boldsymbol{X},t}(a_j) = \frac{1}{N_s} \sum_{i=t}^{N_s+t-1} W^2_{a_j,i}.$$

We chose a window of $N_s = 12$ months since the year is the natural period of geophysical processes occurring across seasons, like temperature and rain. We also considered using smoothing windows of greater width but the overall pattern remained the same. The resulting time-dependent wavelet variances are reported in Figs. 9, 10, 11, 12, and 13. While Figs. 3, 4, 5, and 6 allow us to investigate the changes in the mode of variability, from Figs. 9, 10, 11, 12, and 13 we may get insights into the changes of the magnitude of the variability across the last 160 years. We see that for rain intensity the variability has increased in the last 30 years, both considering the one month scale (responsible of the highest variability, Fig. 9) and the seasonal scale (Fig. 10). On the contrary, the temperature series show a decrease in variability in the last 30 years. For temperature, the highest variability is found during the period 1930-1960. This confirms that the minimum, the maximum and the temperature range in the last 50 years fluctuate less across seasons while the monthly and the seasonal cumulative precipitation depth is much more variable than before.

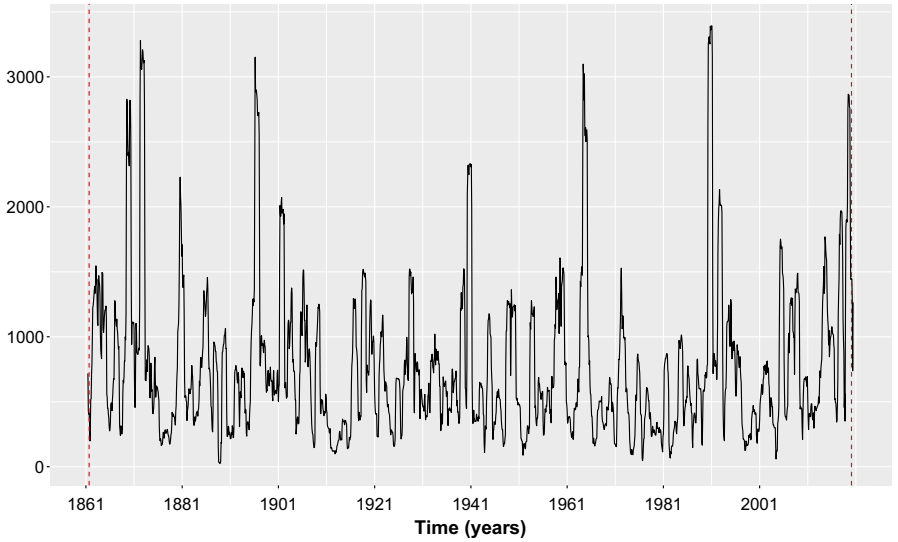

Fig. 9 Time dependent wavelet variance of *PMM*—scale 1 month. The dashed vertical lines represent areas affected by boundary effects

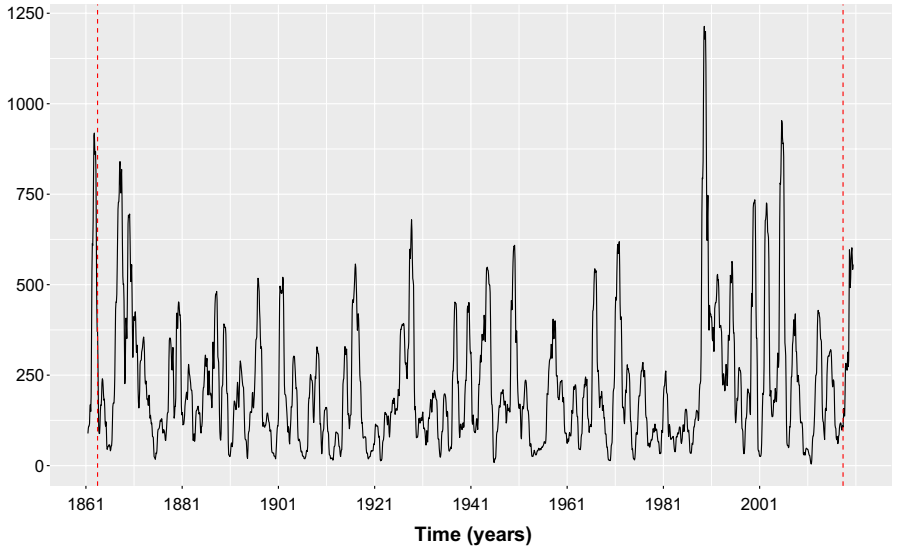

Fig. 10 Time dependent wavelet variance of *PMM* (scale 4 months). The dashed vertical lines represent areas affected by boundary effects

3.3 Continuous wavelet transform

Figures 14, 15, 16, and 17 show the wavelet power spectra obtained with continuous wavelet analysis (Eq. 13). The vertical axis reports the wavelet scale (in

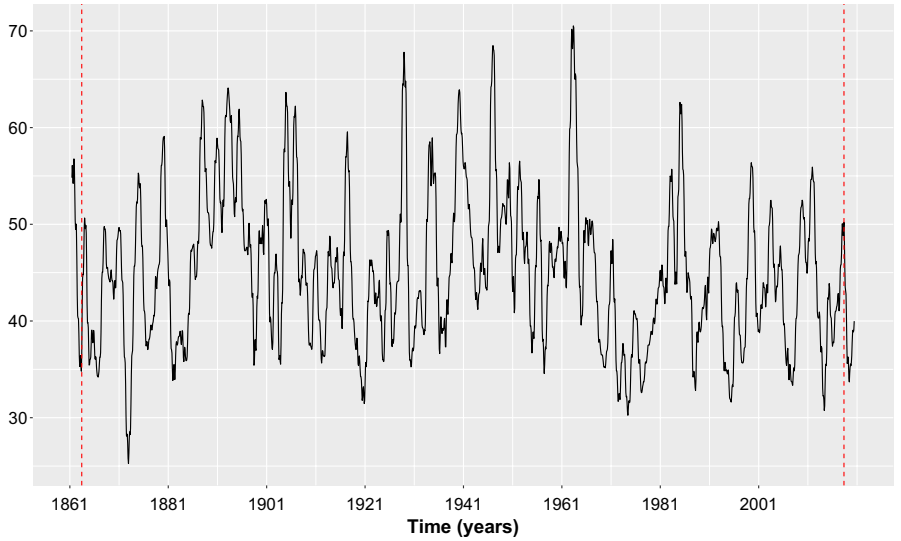

Fig. 11 Time dependent wavelet variance of *Tmin* (scale 4 months). The dashed vertical lines represent areas affected by boundary effects

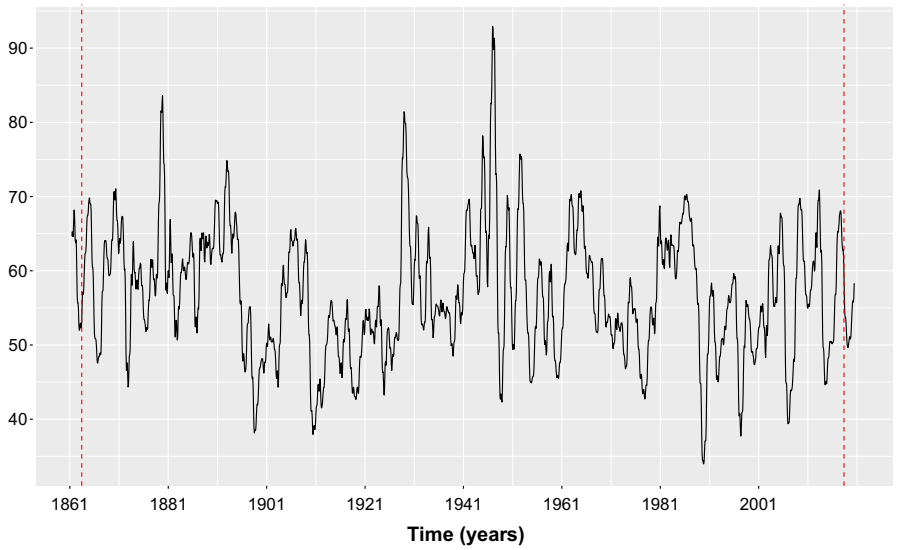

Fig. 12 Time dependent wavelet variance of *Tmax* (scale 4 months). The dashed vertical lines represent areas affected by boundary effects

years) while the horizontal axis is time (in years). The colour code for power ranges from dark blue (low values) to dark red (high values). The superimposed white area indicates the cone of influence that delimits the region influenced

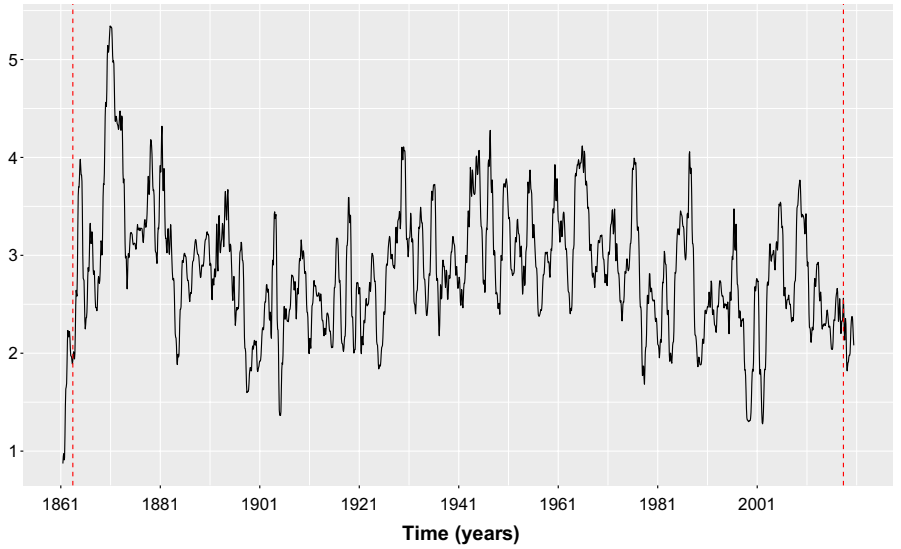

Fig. 13 Time dependent wavelet variance of *Trange* (scale 4 months). The dashed vertical lines represent areas affected by boundary effects

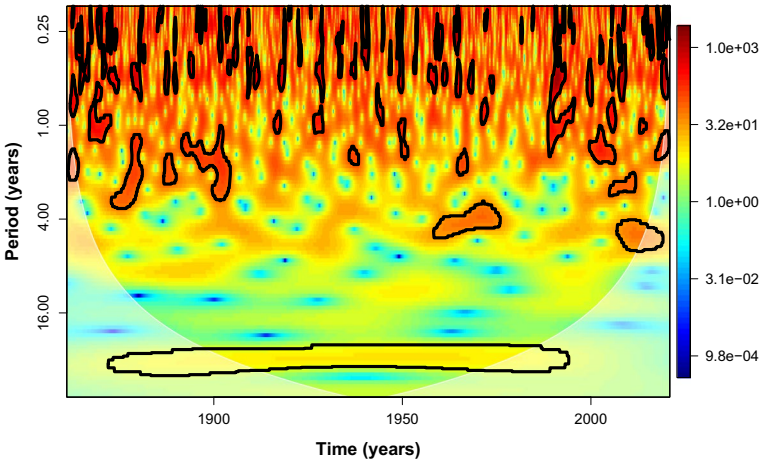

Fig. 14 Wavelet power spectrum of cumulated *PMM*

by edge effects. The thick black contours indicate areas (i.e. patches) significant at the $\alpha = 5\%$ level (following the cumulative area-wise testing by Schulte (2019)). P-values associated with values within the contours are less than 5%. The analysis reveals a single persistent mode of variability of one year within the whole considered period, for temperature. It seems that temperature is not

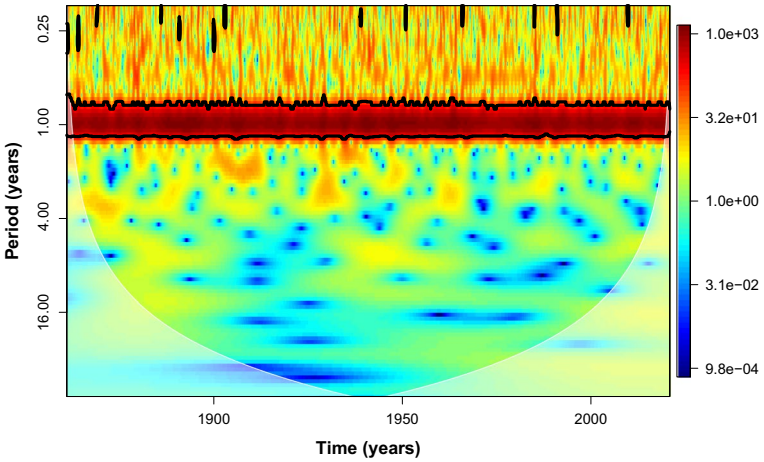

Fig. 15 Wavelet power spectrum of *Tmin*

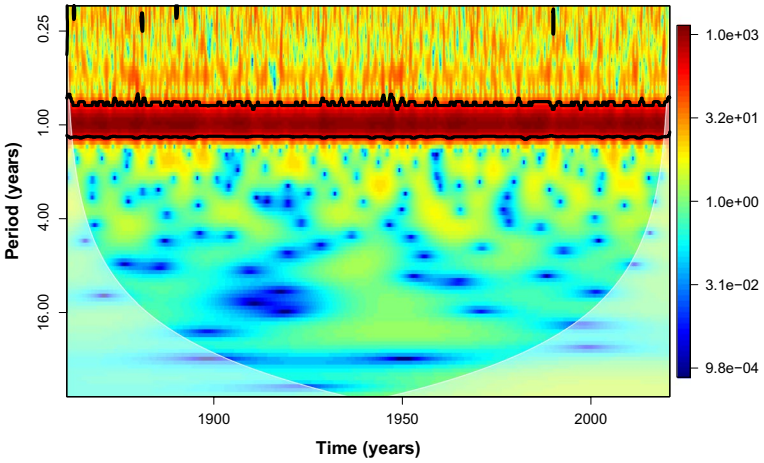

Fig. 16 Wavelet power spectrum of *Tmax*

affected by transient features in annual or multi-annual scales. On the contrary, for the rain there clearly exists a 32-year mode of variability that ends around 1980 (without considering the cone of influence), suggesting a potential change in the process of generating rain at that time. Significant patches at scales of 2 and 4 years before 1900 and after 1950, respectively, seem to be associated with singularity-like time domain features rather than periodicities, since they are intermittent.

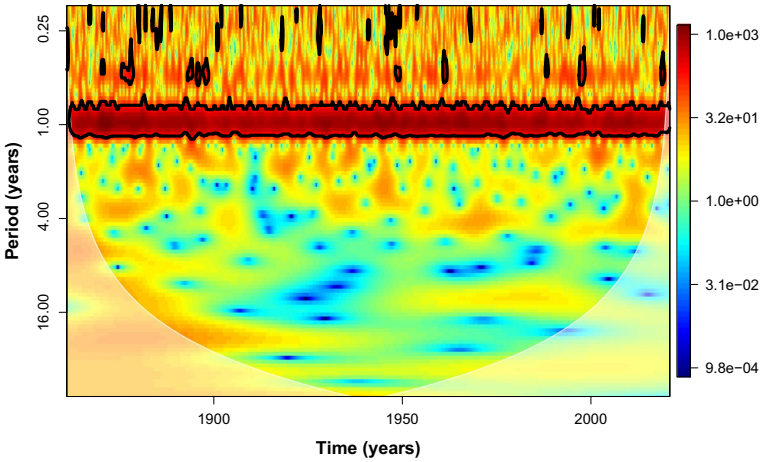

Fig. 17 Wavelet power spectrum of *Trange*

3.4 Wavelet coherence

The analysis of the coherence (Eq. 16) for two time series reveals areas with high common power. The value of the wavelet coherence can be thought of as a localized correlation coefficient in a time-frequency domain: its value in the [0, 1] range provides information about how strong the association between the two series is, at each time point and time scale. The phase difference provides a measure of the lag difference between the two series at each time and scale. We can think about it as a suggestion of causality: if the phase difference is positive, it is the first series leading the second, and the other way around if the phase difference is negative. In the outcome, as for the power spectrum, the superimposed white area indicates the cone of influence, while thick black contours enclose areas (i.e. patches) significant at the $\alpha = 5\%$ level following the cumulative area-wise test.

The top panels in Figs. 18, 19, and 20 show that an intermittent strong (significant) annual association between temperature and rain is present from 1861 until the year 2020. A significant inter-annual association is also found at higher scales but again, it is not constant over time. For *Tmax*, it is particularly strong in the last 20 years on a scale of 28 years, and on a scale of 16 years over the period 1930–2000. The latter relationship is also found for *Tmin*. On the other hand, *Trange* shows a stronger (yet intermittent) relationship with rain that *Tmin* or *Tmax* on scales of 0.5 years and 2-6 years.

The bottom panels in Figs. 18, 19, and 20 show the phase difference. For ease of interpretation, we have added arrows wherever the coherence is above 0.8. It can be seen that the prevalent type of relationship, regardless of the scale, time period and couple of variables, is asymmetric, with temperature leading precipitation and not the other way around. This result can be generalized to a global scale, suggesting that global warming influences the other climatic variables.

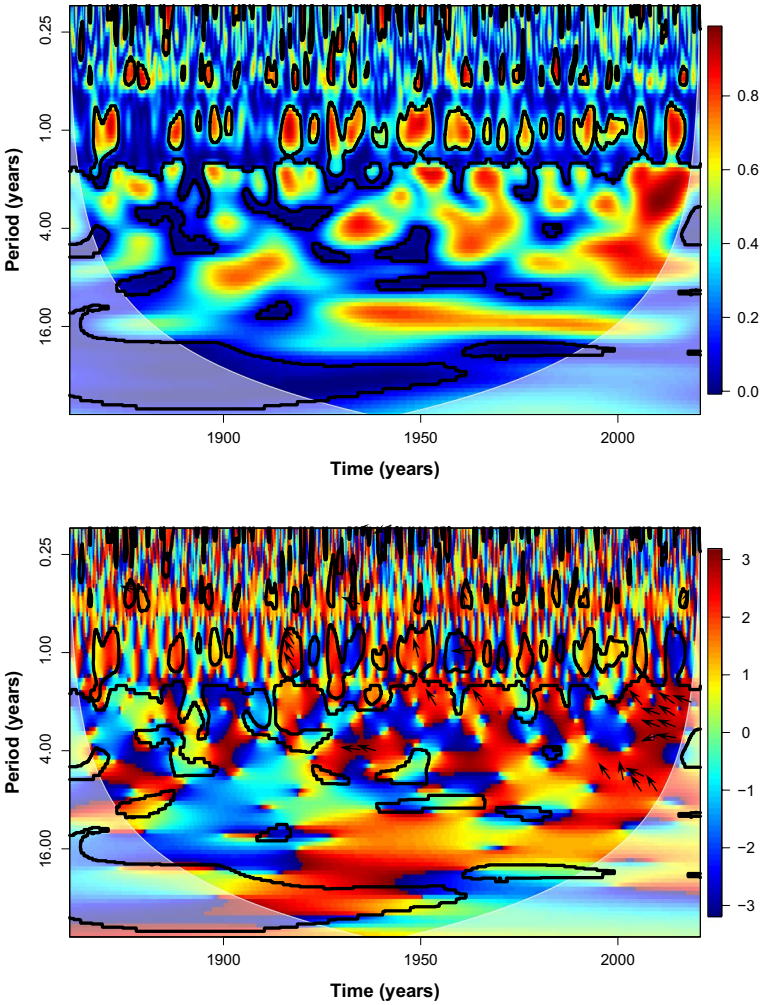

Fig. 18 Wavelet coherence (top) and phase (bottom) between *Tmax* and *PMM*

4 Discussion and Conclusions

Although it is commonly recognized that the mean air temperature is related to the increase in global carbon dioxide concentration, the dynamics of local trends due to local weather variables such as precipitation depth or due to local development remain unclear. Explaining the characteristic of local climate variables and the relationships among them is an important challenge emphasized by the increasing evidence that several ecological processes are affected by local climatic fluctuations. In this study, monthly series of air temperature and precipitation depth are examined over the period of time from 1861 to 2020, and a systematic analysis taking into account the essential features of non stationarity and time scale dependence is

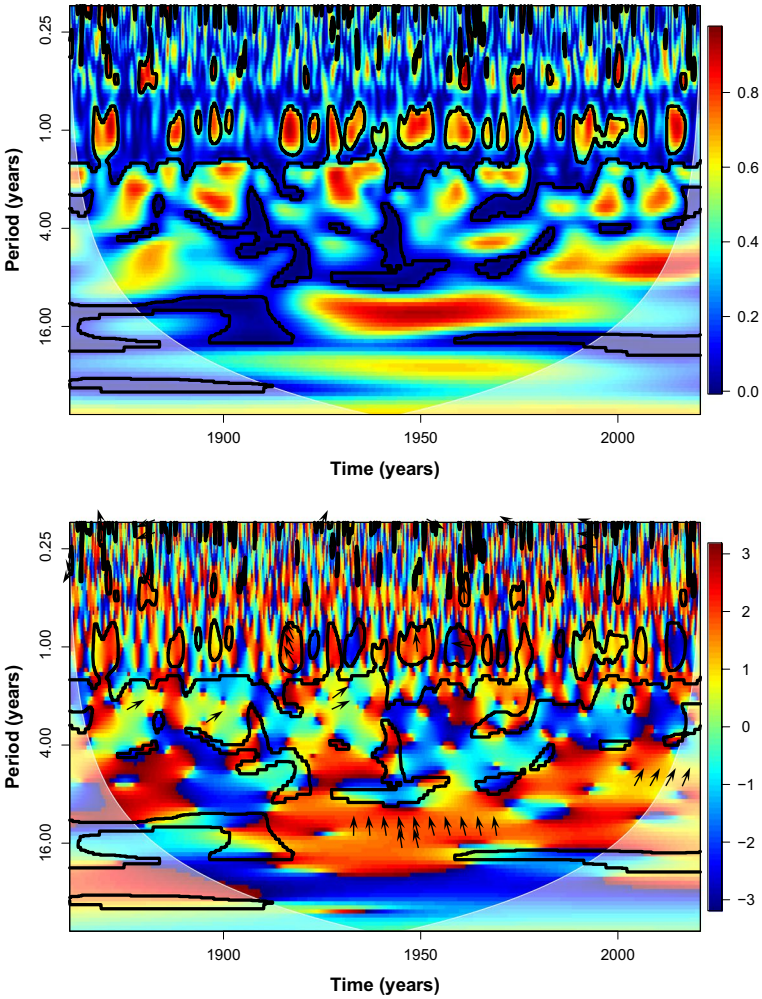

Fig. 19 Wavelet coherence (top) and phase (bottom) between *Tmin* and *PMM*

presented. Data are particularly relevant since long time series of observed and not reconstructed climatic variables are scarce in literature. Advanced statistical tools combining time and frequency domain, such as wavelet analysis are used to determine and compare the internal variability of the series for different scales of time and to study the long-term patterns and the relationships between temperature and precipitation. Analysis of results suggests that the main periodic component leading the variability is one month for precipitation and 4 months for temperature, with a different cycling dynamic over the period 1861–2020 in rain and temperature range, and similar cycling dynamic in minimum and maximum temperature. There appears to be a marked change in the behavior of the long-term trend around 1981 for both rain and temperature. This marked change in the dynamic of the evolution of both

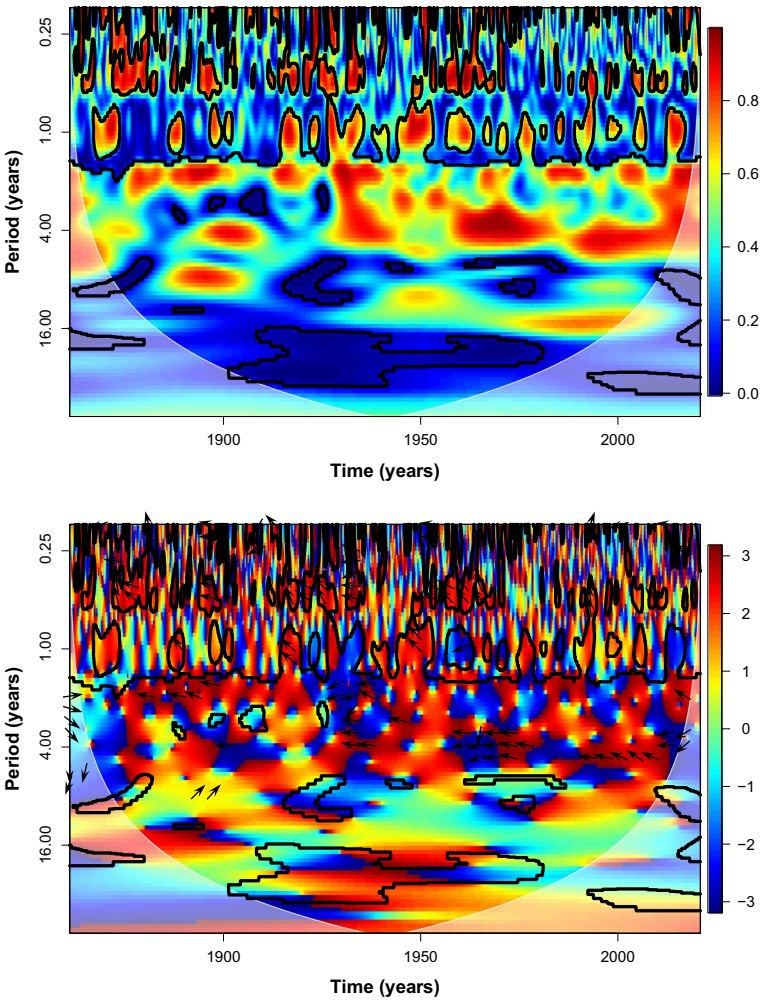

Fig. 20 Wavelet coherence (top) and phase (bottom) between *Trange* and *PMM*

climatic variables can be associated with endogenous or exhogenous mechanisms such as local or global development (global CO_2, anthropogenic heating of urban areas). While rain shows the highest variability in the last two decades, temperature exhibits peaks of variability within the time interval 1930-1960. Within the same period, the relationship between temperature and precipitation is statistically significant considering multi-annual periods of about 16 years. From 2000, the association is highly significant considering multi-annual periods of 2–4 years. There is a strong significant relationship between temperature and precipitation on a yearly cycle but it is not constant over the time period under study. An important finding of this study is the different pattern of the minimum and maximum temperatures and the monthly average of daily range temperature in the last 50 years, consistent with recent works

showing how climate change mostly influences temperature range (Kalnay and Cai 2003; Hua et al. 2008).

In conclusion, the present study highlights the following key points. Changes in temperature maximum and minimum values display different behavior than changes in temperature range. Temperature and precipitation display different timescales of the periodic components and persistent main mode and variances changing in time. Wavelet coherence analysis shows that the relationship between temperature and precipitation evolves in time and suggests that it is temperature driving rainfall and not the other way around.

Acknowledgements The research reported in the present paper was supported by Fondazione Cassa di Risparmio di Modena through the Grant 2018-0093, by the University of Modena and Reggio Emilia through the Grant FAR 2020 Mission Oriented, and by the European Union NextGenerationEU/NRRP, Mission 4 Component 2 Investment 1.5, Call 3277 (12/30/2021), Award 0001052 (06/23/2022), under the Project ECS00000033 "Ecosystem for Sustainable Transition in Emilia-Romagna," Spoke 6 "Ecological Transition Based on HPC and Data Technology." The authors thank the anonymous reviewer for comments that led to improvements in the manuscript.

Data availability The datasets generated during and/or analyzed during the current study are available from the corresponding author on reasonable request.

Declarations

Conflict of interest The authors declare no conflicts of interest relevant to this study.

References

Akansu AN, Smith MJ (1995) Subband and wavelet transforms: design and applications, vol 340. Springer, New York

Akansu AN, Haddad RA, Caglar H (1992) Multiresolution signal decomposition: transforms, subbands, and wavelets. MA Academic Press, Boston

Aldrich E (2020) Wavelets: functions for computing wavelet filters, wavelet transforms and multiresolution analyses. R package version 0.3-0.2. https://CRAN.R-project.org/package=wavelets

Beaulieu C, Killick R, Ireland D, Norwood B (2020) Considering long-memory when testing for change-points in surface temperature: a classification approach based on the time-varying spectrum. Environmetrics 31(1):2568

Boucher O, Reddy MS (2008) Climate trade-off between black carbon and carbon dioxide emissions. Energy Policy 36(1):327–343

Braganza K, Karoly DJ, Hirst AC, Mann ME, Stott PA, Stouffer RJ, Tett SFB (2003) Simple indices of global climate variability and change: part I, variability and correlation structure. Clim Dyn 20:491–502

Braganza K, Karoly DJ, Arblaster JM (2004) Diurnal temperature range as an index of global climate change during the twentieth century. Geophys Res Lett **31**. https://doi.org/10.1029/2004GL01999

Broecker W (2012) The carbon cycle and climate change: memoirs of my 60 years in science. Geochem Perspect 1(2):221–340

Cazelles B, Chavez M, Berteaux D, Menard F, Vik JO, Jenouvrier S, Stenseth NC (2008) Wavelet analysis of ecological time series. Oecologia 156:287–304

Chatfield JR (1989) The analysis of time series: an introduction. Chapman and Hall, London

Chui CK (1992) An introduction to wavelets. Academic Press, Cambridge

Dai A, Trenberth KE, Karl TR (1999) Effects of clouds, soil moisture, precipitation and water vapor on diurnal temperature range. J Clim 12:2451–2473
Daubechies I (1988) Orthonormal bases of compactly supported wavelet. Commun Pure Appl Math 41(7):909–946
Daubechies I (1992) Ten lectures on wavelets. SIAM monographs, Philadelphia
De Laat ATJ, Maurellis AN (2004) Industrial Co2 emissions as a proxy for anthropogenic influence on lower tropospheric temperature trends. Geophys Res Lett **31(5)**
Donoho DL, David L, Johonstone JM (1994) Ideal spatial adaptation by wavelet shrinkage. Commun Pure Appl Math 81(3):425–455
Easterling DR, Peterson TC, Karl TR (1996) On the development and use of homogenized climate data sets. J Clim 9:1429–1434
Easterling DR, Horton B, Jones PD et al (1997) Maximum and minimum temperature trends for the globe. Science 227:364–367
Elayouty A, Scott M, Miller C, Waldron S, Franco-Villoria M (2016) Challenges in modeling detailed and complex environmental data sets: a case study modeling the excess partial pressure of fluvial CO_2. Environ Ecol Stat 23(1):65–87
Gallegati M (2018) A systematic wavelet-based exploratory analysis of climatic variables. Clim Change 148:325–338
Gambis D (1992) Wavelets transform analysis of the length of the day and the el Nino southern oscillation variations ate intra-seasonal and inter-annual time scale. Ann Geophys 10:429–437
Gao W, Li BL (1992) Wavelets analysis of coherent structure at the atmosphere forest interface. J Appl Meteor 32:1717–1725
Gouhier TC, Grinsted A, Simko V (2021) R package biwavelet: conduct univariate and bivariate wavelet analyses (Version 0.20.21). https://github.com/tgouhier/biwavelet
Grinsted A, Moore JC, Jevrejeva S (2004) Application of the cross wavelet transform and wavelet coherence to geophysical time series. Nonlinear Process Geophys 11:561–566. https://doi.org/10.5194/hess-20-3183-2016
Hansen JE, Lebedeff S (1987) Global trends of measured surface air temperature. J Geophys Res 92:13345–13372
Hansen J, Johnson D, Lacis A, Lebedeff S, Lee P, Rind D, Russel G (1981) Climate impact of increasing atmospheric carbon dioxide. Science 213(4511):957–966
Hansen J, Ruedy R, Sato M, Lo K (2010) Global surface temperature range. Rev Geophys. https://doi.org/10.1029/2010RG000345
Hua L, Ma Z, Guo W (2008) The impact of urbanization on air temperature across china. Theoret Appl Climatol 93(3):179–194
Kalnay E, Cai M (2003) Impact of urbanization and land-use change on climate. Nature 423(6939):528–531
Karl B, Karoly DJ, Arblaster JM (2004) Diurnal temperature range as an index of global climate change during the twentieth century. Geophys Res Lett 31:13217
Korkas KK, Fryzlewicz P (2017) Multiple change-point detection for non-stationary time series using wild binary segmentation. Stat Sin 27:287–311
Kumar P, Foufoula-Georgiou E (1993) A new look at rainfall fluctuations and scaling properties of spatial rainfall using orthogonal wavelets. J Appl Meteor 32:209–222
Lau KM, Weng H (1995) Climatic signal detection using wavelet transform: how to make a time Serie Sing. Bull Am Meteorol Soc 76:2391–2402
Leathers DJ, Palecki MA, Robinson NA, Dewey KF (1998) Climatology of the daily temperature range annual Cicle in the united states. Clim Res 9:197–211
Makowski K, Wild M, Ohmura A (2008) Diurnal temperature range over Europe between 1950 and 2005. Atmos Chem Phys 8:6483–6498
Mallat S (1999) A wavelet tour of signal processing. CA Academic, San Diego
Maraun D, Kurths J (2004) Cross wavelet analysis: significance testing and pitfalls. Nonlinear Process Geophys 11:505–514. https://doi.org/10.5194/npg-11-505-2004
Maraun D, Kurths J, Holschneider M (2007) Non-stationary gaussian processes in wavelet domain: definitions, estimation and significance testing. Phys Rev E. https://doi.org/10.1103/PhysRevE.75.016707

McGonigle ET, Killick R, Nunes MA (2022) Trend locally stationary wavelet processes. J Time Ser Anal 43(6):895–917
Mi X, Rend Z, Ouyang H, Wei W, Ma K (2005) The use of the Mexican hat and the Morlet wavelets for detection of ecological patterns. Plant Ecol 179, 1–19. https://doi.org/10.1007/s11258-004-5089-4
Nason G (2013) A test for second-order stationarity and approximate confidence intervals for localized autocovariances for locally stationary time series. J R Stat Soc 879–904
Nason GP, Von Sachs R, Kroisandt G (2000) Wavelet processes and adaptive estimation of the evolutionary wavelet spectrum. J R Stat Soc 62(2):271–292
Ozbay N, Toker S (2021) Prediction framework in a distributed lag model with a target function: an application to global warming data. Environ Ecol Stat 28:87–134. https://doi.org/10.1007/s10651-020-00477-x
Percival DB, Walden AT (2000) Wavelet methods for time series analysis. Cambridge University Press, Cambridge
Qu M, Wan J, Hao X (2014) Analysis of diurnal air temperature range change in the continental united states. Weather Clim Extremes 4:86–95. https://doi.org/10.1016/j.wace.2014.05.002
R Core Team (2021) R: a language and environment for statistical computing. R Foundation for Statistical Computing, Vienna, Austria, R Foundation for Statistical Computing. https://www.R-project.org/
Ruskal MB, Beylkin G, Coifman R, Daubechies I, Mallat S, Meyer Y, Raphael L (1992) Wavelets and their applications. Jones and Bartlett, Burlington
Schulte JA (2016) Cumulative areawise testing in wavelet analysis and its application to geophysical time series. Nonlinear Process Geophys 23:45–57. https://doi.org/10.5194/npg-23-45-2016
Schulte JA (2016) Wavelet analysis for non-stationary, nonlinear time series. Nonlinear Process Geophys 23:257–267. https://doi.org/10.5194/npg-23-257-2016
Schulte JA (2019) Statistical hypothesis testing in wavelet analysis: theoretical developments and applications to Indian rainfall. Nonlinear Process Geophys 26:91–108
Schulte JA, Duffy C, Najjar RG (2015) Geometric and topological approaches to significance testing in wavelet analysis. Nonlinear Process Geophys 22:139–156. https://doi.org/10.5194/npg-22-139-2015
Simmons AJ, Willett KM, Jones PD, Thorne PW, Dee DP (2010) Low-frequency variations in surface atmospheric humidity, temperature, and precipitation: inferences from reanalyses and monthly gridded observational data sets. J Geophys Res. https://doi.org/10.1029/2009JD012442
Stone DA, Weaver AJ (2002) Daily maximum and minimum temperature trends in a climate model. Geophys Res Lett 29(9):1356. https://doi.org/10.1029/2001GL014556
Stone DA, Weaver AJ (2003) Factors contributing to diurnal temperature range trends in twentieth and twenty-first century simulations of the CCMA coupled model. Clim Dyn 12:2451–2473
Sun D, Pinker R, Kafatos M (2006) Diurnal temperature range over the united states: a satellite view. Geophys Res Lett 33:05705
Sutton R, Suckling E, Hawkins E (2015) What does global mean temperature tell us about local climate? Philosophical transactions. Ser A Math Phys Eng Sci. https://doi.org/10.1098/rsta.2014.0426
Thompson DWJ, Wallace JM, Jones PD, Kennedy JJ (2009) Identifying signatures of natural climate variability in time series of global-mean surface temperature: methodology and insights. J Clim 22:6120–6141
Torrence C, Compo GP (1998) A parctical guide to wavelet analysis. Bull Am Meteorol Soc 79:61–78
Torrence C, Webster P (1999) Interdecadal changes in the Esno-Monsoon system. J Clim 12:2679–2690
Woody J, Lu Q, Livsey J (2020) Statistical methods for forecasting daily snow depths and assessing trends in inter-annual snow depth dynamics. Environ Ecol Stat 27:609–628. https://doi.org/10.1007/s10651-020-00461-5

Authors and Affiliations

Isabella Morlini[1] · Maria Franco-Villoria[2] · Stefano Orlandini[3]

✉ Isabella Morlini
isabella.morlini@unimore.it

Maria Franco-Villoria
maria.francovilloria@unimore.it

Stefano Orlandini
stefano.orlandini@unimore.it

[1] Department of Communication and Economics, University of Modena and Reggio Emilia, Reggio Emilia, Italy

[2] Department of Economics Marco Biagi, University of Modena and Reggio Emilia, Modena, Italy

[3] Department of Engeneering Enzo Ferrari, University of Modena and Reggio Emilia, Modena, Italy